Interactions of Basic Amphiphilic Peptides with Dimyristoylphosphatidylcholine Small Unilamellar Vesicles: Optical, NMR, and Electron Microscopy Studies and Conformational Calculations

J. A. Reynaud,* J. P. Grivet,‡ D. Sy,‡ and Y. Trudelle

Centre de Biophysique Moléculaire, CNRS, 1A, Avenue de la Recherche Scientifique, 45071 Orleans Cedex 2, France

Received June 29, 1992; Revised Manuscript Received January 11, 1993

ABSTRACT: The interactions of DMPC small unilamellar vesicles with four amphiphilic polypeptides [$(LKKL)_n$, $(LRRL)_n$, $(LKKL)_4$, and $(YKKY)_n$] have been investigated by circular and infrared dichroism, turbidimetry, electron microscopy, and fluorescence, ^1H, and ^{31}P nuclear magnetic resonance spectroscopy. The main results obtained are the following: (1) Well-defined complexes are formed by the association of one amino acid residue with approximately two lipid molecules. (2) In the presence of polypeptides fusions are observed between SUVs when the molar ratio p is less than 0.05, and a clearance effect is observed when p is higher than 0.05. (3) The anchoring sites of the polypeptides on DMPC molecules are the negative phosphate groups through electrostatic interactions with the terminal NH_3^+ of lysine residues. (4) The polypeptides adopt an α-helical conformation with their axis parallel to the membrane surface. The hydrophobic part of the amphiphilic α helix can penetrate the outer lipid leaflet down to the C_5 position. (5) Choline methyl groups are not involved in the interactions between lipid molecules and amino acid residues. (6) Phosphorus atom mobility around the P–O–glycerol bond is strongly reduced whereas that of methylene groups is progressively weakened when going up from C_{13} to C_1. Finally, using modeling and energy calculations a model of possible $Ac(LKKL)_4NHEt$–DMPC SUV complexes is presented.

Interactions of various natural polypeptides with biomembranes play a key role in many biological phenomena and are known to affect both polypeptide and membrane structural organization. A nonexhaustive list of peptides of biological significance in this context is the following: viral protein fragments, cytolytic peptides, several peptide hormones, neuropeptides, serum protein fragments, and signal peptides. Most of these have an important structural feature in common. Their sequence is such that they can potentially form an amphiphilic α helix. In order to give rise to this type of structure, electrically charged hydrophilic residues and hydrophobic residues must be suitably distributed along the sequence (Kaiser & Kezdy, 1987; Taylor & Osapay, 1990; Tamm, 1991).

Up to now, several experimental approaches have been employed for the study of the interactions between polypeptides and membranes or membrane models, and many of them use synthetic polypeptides able to mimic the natural compounds and their biologically relevant activity when interacting with a membrane (Anantharamaiah et al., 1985; Schlegel & Wade, 1985; Ho & De Grado, 1987; Lee et al., 1987; Mihara et al., 1987; Houbre et al., 1988; Ono et al., 1988, 1990; Suenaga et al., 1988; Bruner, 1989; Kono et al., 1990; Takahashi, 1990; Clague et al., 1991; Kato et al., 1991; Lee et al., 1992; Maget-Dana & Trudelle, 1991; Mac Lean et al., 1991; Merulka & Stellwagen, 1991; Mosior & McLaughlin, 1992; Yeagle et al., 1991).

Among the numerous natural peptides forming an amphiphilic α helix in the presence of lipid membranes and generally giving rise to a fusogenic activity, many possess various arrangements of neutral hydrophobic sequences and electrically charged hydrophilic units. At this time the very simple sequence formed of alternating doublets of hydrophobic and hydrophilic residues has not yet been investigated.

In this paper we report on the interaction between dimyristoylphosphatidylcholine small unilamellar vesicles (DMPC SUV) and four synthetic polypeptides having this type of sequence (Reynaud et al., 1990). These are listed in Table I. These polypeptides were chosen for the following additional reasons.

(i) Our investigations were first undertaken using polypeptides I, II, and III which are polydisperse polymers, soluble in water, easy to prepare, and extensively studied as to their conformational properties (Perello et al., 1991; Barbier et al., 1988). The shorter peptide IV of defined length was used to reduce the complexity of the system and to make possible its accurate characterization.

When the ionic strength is increased, they undergo a conformational transition toward an α helix. We will show that a similar behavior is observed in the presence of vesicles. The peptide–vesicle interaction is thus easily followed through its effect on the circular dichroism spectrum, which is quite sensitive to conformational changes.

(ii) Our peptides comprise alternating doublets of hydrophobic and hydrophilic amino acids. Their conformation is therefore quite sensitive to the balance of electrostatic and hydrophobic interactions. Phospholipids are able to shift this balance and change the conformation.

(iii) In the case of the hexadecapeptide $(LKKL)_4$, the periodicity is such that the hydrophobic residues are all located on one side of the helix, while the hydrophilic amino acids are concentrated on the other side; the helix is thus divided into two halves.

(iv) Replacement of the leucine residues by tyrosine moieties provides a convenient chromophore, without seriously dimin-

* Author to whom correspondence should be addressed.
‡ Present address: University of Orléans, Orleans, France.

0006-2960/93/0432-4997$04.00/0

Table I: Characteristics of Free Polymer Samples[a]

no.	polymer	abbreviation	$\bar{M}_n$	M
I	poly(Leu-Arg-Arg-Leu)·2HCl	$(LRRL)_n$	6 300	
II	poly(Tyr-Lys-Lys-Tyr)·2HCl	$(YKKY)_n$	22 000	
III	poly(Leu-Lys-Lys-Leu)·2HCl	$(LKKL)_n$	35 000	
IV	Ac(Leu-Lys-Lys-Leu)$_4$NHEt·8TFA	$(LKKL)_4$		3215

[a] $\bar{M}_n$ denotes the number-average molecular weight, M denotes the molecular weight, and it is assumed that there are two H_2O molecules per lysyl residue.

ishing the tendency toward helix formation in the presence of vesicles.

(v) As shown hereafter, these polypeptides display fusogenic properties on small unilamellar vesicles and therefore can be considered as good models for shedding some light on peptide-induced fusion phenomena between lipid membranes.

In this report, we show that the peptides do indeed interact with the vesicles, with attending formation of an α helix. We address the following questions. What is the nature of the interaction between peptides and vesicles? What is the orientation of the helix with respect to the phospholipid bilayer? Do these synthetic peptides penetrate the bilayer or not?

MATERIALS AND METHODS

(*a*) *Chemicals.* The characteristics of the polymers used in this study are presented in Table I.

Peptide Synthesis. Polypeptides I, II, and III were obtained by condensing the tetrapeptide repeat unit *p*-nitrophenyl ester (Barbier et al., 1988; Trudelle, unpublished results). After removal of the side-chain protecting groups by HBr/TFA, the free polymers thus obtained were dialyzed exhaustively against dilute HCl and water using Spectrapor 3 dialysis tubing (cutoff: 3000).

The polymers were recovered by lyophilization. The hexadecapeptide IV was prepared by solid-phase synthesis using a Boc/Pam resin strategy. Cleavage from the resin was achieved by treatment with ethylamine. After deprotection of lysine side chains by HBr/TFA the free peptide was purified by HPLC on a C18 Lichrospher column (from Merck) using an acetonitrile–water–0.2% TFA gradient system. The pure peptide was then recovered by lyophilization.

Peptide concentrations were determined by weighing, assuming two H_2O molecules per lysyl side chain. This water content, previously determined (Brack & Caille, 1978; Barbier et al., 1988) using similar polypeptides, was checked in the present work by elementary analysis for polypeptides I, III, and IV and by UV spectroscopy for polypeptide II, assuming an extinction coefficient of 2200 at 293.5 nm per tyrosyl residue in 0.2 N NaOH.

The peptide concentrations were obtained by weighing and are expressed either as moles of amino acid residues per liter, C_p, or as the molar ratio

$$p = C_p/(C_p + C_L)$$

where C_L is the phospholipid concentration in moles per liter.

1,2-Dimyristoyl-3-phosphatidylcholine (DMPC)[1] was purchased from Calbiochem and used without further purification.

Carboxyfluorescein (CF) from Sigma was used after recrystallization in ethanol and purification by chromatography on LH20 Sephadex. Purity was checked by HPLC on a C18 reverse-phase column. All other reagents were of analytical grade. All measurements, except those for carboxyfluorescein efflux, were made at 303 K above the T_m of DMPC (297 K).

As a matter of fact, at 303 K, the carboxyfluorescein efflux kinetics was too fast for the measurements to be recorded, and for this reason the 292 K temperature was selected.

(*b*) *Preparation of Small Unilamellar Phospholipid Vesicles (SUV).* Vesicles were obtained by sonicating aqueous DMPC suspensions (33 mg/mL) according to Huang (1969). They were examined by electron microscopy (Siemens Elmiskop 102) after negative staining with 2% sodium tungstate. More than 85% of the vesicles had a diameter between 18 and 25 nm.

(*c*) *Carboxyfluorescein Leakage.* Carboxyfluorescein-(CF-) containing DMPC vesicles were prepared according to Surewicz and Epand (1984) with the following modifications: (i) HEPES was used instead of PIPES; (ii) removal of free CF was performed at 277 K; CF leakage was followed by the fluorescence change at 292 K and pH 7.4 with excitation and emission wavelengths of 490 and 520 nm, respectively, according to Weinstein et al. (1977) and Surewicz and Epand (1984). The percentage of CF released was obtained as follows. The vesicles were disrupted by addition of Triton X-100 to a final concentration of 2%; the resulting fluorescence intensity was taken to indicate that 100% of the dye was set free. The fluorescence time course in the presence of peptide is reported as a percentage of this maximum.

(*d*) *Optical Spectroscopy.* Circular dichroism measurements were performed using a Jobin-Yvon Mark IV dichrograph. Ellipticity is expressed as a mean residue ellipticity $[\theta]$, with the units deg·cm^2·dmol^{-1}. Absorbance measurements were recorded with a Perkin-Elmer lambda 15 spectrophotometer. Fluorescence spectra were recorded on a 3C Jobin-Yvon spectrofluorometer while polarized infrared spectra were obtained with a Perkin-Elmer 297 spectrophotometer, equipped with a wire grid polarizer.

Since the optical dichroic density is proportional to the concentration, circular dichroism could be used to determine the stoichiometry of the peptide–phospholipid interaction. It is assumed that a single complex is formed, according to the general formula

$$AA^{\alpha} + n\mathrm{PL} = [AA^{\alpha}\mathrm{PL}_n]$$

where the superscript α indicates that an amino acid residue (AA) comprised in an α helix is associated with n phospholipid molecules (PL). We then use Job's method (Souchay, 1961) to determine n. Two equimolar ($C_L = C_p = 1.2 \times 10^{-3}$ M in the present case) solutions of peptide and phospholipid were mixed in varying proportions to obtain various final p values. A plot of $[\theta']C_p^2$ versus p exhibited a maximum at $p = p_m$; as shown in Appendix I, n is given by

$$n = (1 - p_m)/p_m$$

IR dichroism was measured at an incidence angle of 60°. The light was linearly polarized either perpendicular (absorbance $A_\perp$) or parallel (absorbance $A_\parallel$) to the plane of incidence, as described earlier (Nabedryk et al., 1982). Fifty

[1] Abbreviations: DMPC, 1,2-dimyristoyl-3-phosphatidylcholine; HEPES, 4-(2-hydroxyethyl)-1-piperazineethanesulfonic acid; LUV, large unilamellar vesicle; PIPES, 1,4-piperazinediethanesulfonic acid; PL, phospholipid; SUV, small unilamellar vesicle; CF, carboxyfluorescein; CD, circular dichroism; IR, infrared; NMR, nuclear magnetic resonance; OD, optical density; TFA, trifluoroacetic acid.

[2] $[\theta']$ denotes the corrected dichroic density which represents the effective helical content for $(LKKL)_4$.

microliters of a 4.92×10^{-2} M vesicle suspension containing $(LKKL)_4$ at a suitable concentration was applied to a 20-mm-diameter fluorine disk. Stacking of the vesicles parallel to the disk plane was achieved by slow air-drying at room temperature (Nabedryk et al., 1982). The dichroic ratio D is defined as

$$D = A_{\parallel}/A_{\perp}$$

Measurements were made at 1660 cm^{-1}, corresponding to the amide I band of the peptide. Assuming that the molecule is helical, that the transition moment makes an angle α with the helix axis, D can easily be computed (Bamford et al., 1956; Appendix II) for two simple limiting cases, helices randomly oriented in the disk plane (case I) or helices normal to the disk plane (case II), with the following results:

$$\text{case I: } D_{\text{I}} = \frac{\langle A_{\parallel}\rangle}{\langle A_{\perp}\rangle} = \frac{(3\cos^2\alpha - 1)\cos^2 r + 2\sin^2\alpha}{1 + \cos^2\alpha}$$

$$\text{case II: } D_{\text{II}} = \frac{\langle A_{\parallel}\rangle}{\langle A_{\perp}\rangle} = 2\sin^2 r \cot^2\alpha + \cos^2 r$$

In these formulas, r is the angle of the light beam with the disk normal, inside the sample; it may be computed from the angle of incidence i and the refractive index n (1.55) using Descartes' law; $\sin i = n \sin r$. For the commonly accepted $\alpha = 39°$, $i = 60°$, and $n = 1.55$ (Nabedryk et al., 1982), $D_{\text{I}} = 0.85$ and $D_{\text{II}} = 1.575$.

(*e*) *NMR Spectroscopy.* Spectra were recorded on a Bruker AM 300 instrument at 300 MHz (proton) or 121.4 MHz (phosphorus). For proton work, 5-mm-diameter tubes were used. The chloroform signal of a sealed capillary (set at 7.2 ppm) was used as a frequency and intensity standard. The residual HDO signal was attenuated by low-power presaturation. About a hundred scans were accumulated, using 8K data points and a 12-ppm spectral window. A 1-Hz exponential filter was used before Fourier transformation. For ^{31}P spectroscopy, either 5- or 10-mm tubes were used, again with an external reference (methylenediphosphonic acid solution in water, 0.1 M, pH = 8). Some 2000 scans were accumulated, using 2K points, for a 70-ppm spectral window; broad-band proton decoupling had no effect on spectra. The free induction decays were multiplied by an exponential function, equivalent to a 20-Hz broadening, before transformation. The temperature was held at 303 K for all spectra.

(*f*) *Conformational Calculations.* Complexes were designed using Sybyl modeling (Tripos Associates, Inc.). In each case the lipid alkyl chains normal to the helix axis were brought near the anchoring site, and constraints of distance between phosphorus and nitrogen atoms were set within a range 2.5–4.5 Å. The corresponding energies were computed with the Tripos force field (Clark et al., 1989) and a cutoff length of 8 Å. For the electrostatic energy term, Gasteiger–Hückel atomic charges were used, and the permittivity ϵ was a function of the interatomic distance in order to simulate the polar environment. We tested as well both the value of 4 for the permittivity (as in the Amber force field, which gave comparable energy values) and a macroscopic permittivity decreasing along the alkyl chains from 30 to 4 (Brasseur & Ruysschaert, 1986). In that calculation the electrostatic energy terms were lessened, but the relative energies of the complexes being studied were in the same stability order and the final configurations were similar to those obtained with ϵ as a function of the interatomic distance.

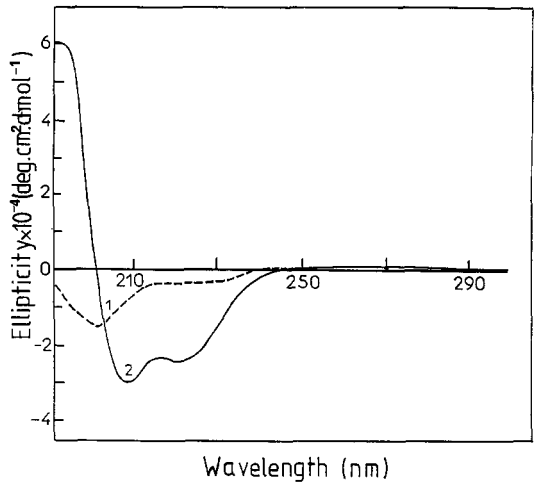

FIGURE 1: Circular dichroism spectra of $(LRRL)_n$: (- - -) $c = 1.5 \times 10^{-2}$ M in pure water; (—) $c = 5.74 \times 10^{-3}$ M in 0.0492 M DMPC vesicle suspension.

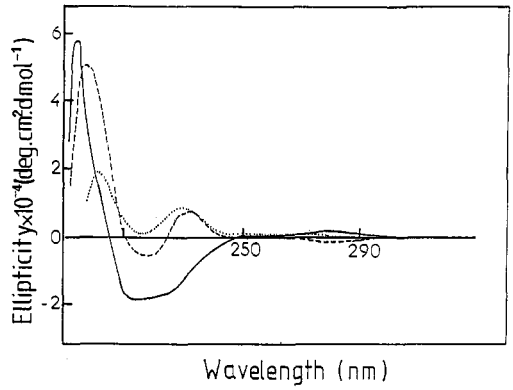

FIGURE 2: Circular dichroism spectra of $(YKKY)_n$: (• • •) $c = 5.5 \times 10^{-3}$ M in pure water; (- - -) $c = 5.5 \times 10^{-3}$ M in 0.1 M NaCl; (—) $c = 5.5 \times 10^{-3}$ M in 0.0492 M DMPC vesicle suspension.

RESULTS AND DISCUSSION

Since the four polypeptides listed in Table I behave similarly in the presence of DMPC vesicles, the experimental results presented will refer to either polypeptide.

(*a*) *Circular Dichroism.* In the presence of DMPC vesicles, the CD spectra of peptides I, III, and IV displayed two minima at 208 and 222 nm (Figure 1). These features were also observed for the free peptides at high ionic strength (Barbier et al., 1988) and are characteristic of an α-helical conformation.

In the case of the hexadecapeptide $(LKKL)_4$ for p values less than 0.2, the helix content calculated from the formula of Greenfield and Fasman (1969) equaled 100%. This result gives evidence for the formation of a complex between DMPC vesicles and polypeptides where the electrostatic interactions between the negatively charged phosphate groups and the protonated lysine residues play a crucial role in the binding process.

In this context the CD spectra of $(YKKY)_n$ are of special interest. It is known that, in tyrosine-rich peptides (Woody, 1978), the CD contribution of the aromatic side chains is highly dependent upon their orientation. For instance, in a 0.1 M NaCl solution, the CD spectrum of $(YKKY)_n$ does not resemble that of an α helix; nevertheless, by comparison with the spectra of analogous tyrosine-rich peptides (Trudelle, 1975), one can ascertain that $(YKKY)_n$ is indeed in a helical conformation. In contrast, Figure 2 shows that, in the presence of vesicles, the tyrosyl CD signal is practically abolished,

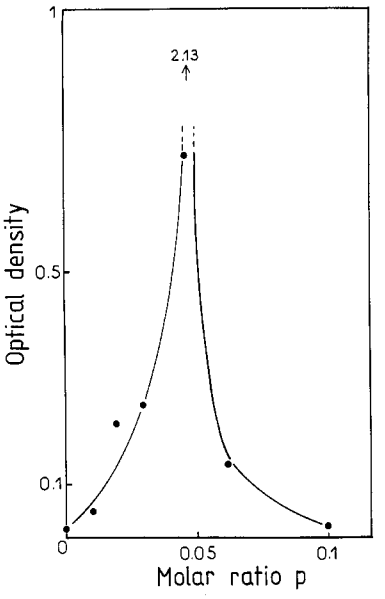

FIGURE 3: $(LKKL)_4$ turbidity dependence with molar ratio. Optical density was measured at 400 nm.

leaving only a classical α-helix-like spectrum. This means that the orientation of the aromatic rings is completely modified and that the interaction between residues i and $i+4$ vanishes (Woody, 1978). Such a result strongly suggests that lipid chains could be located between the aromatic rings and could prevent them from stacking.

(*b*) *Turbidity*. Changes in vesicle size due to aggregation and/or fusion can be monitored by measuring the turbidity (or absorbance OD) of the dispersion. If the mean radius $\langle r \rangle$ of the diffusing particles remains less than the wavelength, then turbidity is roughly proportional to $\langle r \rangle^3$ and can be used as a sensitive measure of particle size distribution. The variation of OD_{400} as a function of p, in the case of $(LKKL)_4$, is shown in Figure 3. The absorbance increases and goes through a very sharp maximum centered around $p = 0.05$, corresponding to a strong increase in particle sizes. Such a behavior should be related to some aggregation or fusion phenomena.

The maximum is immediately followed by a steep decrease; this clearing effect is visible with the naked eye. The turbidity maximum occurs for p close to 0.05, within a range of ± 0.04 unit depending on the considered peptide.

(*c*) *Electron Microscopy*. In order to gain further information concerning the increasing turbidity and clearing effects, electron microscopy measurements were simultaneously undertaken: four such photographs are shown in Figure 4. The p values were chosen to correspond to both the rising and falling part of the turbidity curve. Figure 4a shows a vesicle dispersion in pure water; Figure 4b, for $p = 0.02$, displays a group of aggregated vesicles, which are apparently undergoing fusion. Figure 4c ($p = 0.05$) represents a large unilamellar vesicle (LUV), which results from the fusion of several smaller vesicles. In Figure 4d ($p = 0.2$), small irregular particles are seen; they result from the fragmentation of the previous large vesicles, and their formation corresponds to the clearing of the solution. The apparent aggregation observed on the electron microscopy photograph corresponded to an artifact resulting from the dehydration of the preparation on the grid during the electron microscopy observation.

(*d*) *Carboxyfluorescein Leakage*. The leakage of carboxyfluorescein encapsulated in the vesicles was used to investigate the perturbation brought about by the peptide on the bilayer. The efflux of CF was detected by an increase of the fluorescence intensity (decrease of quenching) upon dilution of the dye in the bulk aqueous phase. The fluorescence time course after addition of a minute amount of peptide is shown in Figure 5. Both $(LKKL)_4$ and $(YKKY)_n$ are seen to be highly effective in disrupting the vesicles.

We have mainly reported results of several macroscopic measurements, which all indicate that peptides interact strongly with vesicles. It was felt important to investigate this interaction at the microscopic level. We therefore turned to spectroscopic techniques to gain further insights.

(*e*) *Stoichiometry of the Lipid–Peptide Interaction*. The variation of the mean residue ellipticity $[\theta]$ at 208 nm with p is shown in Figure 6 for $(LKKL)_n$ and $(LKKL)_4$. The curves obtained for both polypeptides are very similar and display a sigmoidal shape. We can note that $(LKKL)_4$ was fully helical within the p range 0–0.15, whereas the ellipticity content of $(LKKL)_n$ was 90% only as obtained from the formula of Greenfield and Fasman (1969). The p dependence of the $(LKKL)_4$ corrected dichroic density θ' is displayed in Figure 7. The curve goes through a maximum for $p = p_m = 0.33$. According to the relation $n = (1 - p_m)/p_m$, derived in Appendix I, $n = 2 \pm 0.4$. It should be kept in mind that n represents an average complexation number; this means that for the complex between $(LKKL)_4$ and DMPC SUV the average number of lipids involved in the interaction is about 32 ± 7.

(*f*) *Infrared Dichroism Study of Ac(LKKL)$_4$NHEt in Vesicles*. When DMPC vesicles suspended in water are spread on a plane and slowly air-dried, hydrocarbon chains become orientated nearly parallel to the normal of the plane, as previously shown by Nabedryk et al. (1982) by IR dichroism. We have assumed that during this drying process $(LKKL)_4$ in the presence of liposomes is expected to suffer no significant rearrangement and to adopt two possible helical orientations either parallel or perpendicular to the bilayer plane. IR dichroism experiments were undertaken to discriminate between these two possible orientations. The IR spectra for both $A_\parallel$ and $A_\perp$ are presented in Figure 8.

The only amide band I was used (insert of the Figure 8) because amide band II (weakly dichroic) was overlapped by the absorption of some water probably tightly bound to lysine side chains.

At a low peptide/lipid ratio ($p = 0.09$) for which phospholipid molecules are still arranged as a bilayer and $(LKKL)_4$ as an α helix, the IR absorption amide band I at 1660 cm^{-1} showed a dichroic ratio D of 0.84. This result argues strongly in favor of a parallel orientation. Besides, this latter conclusion could be expected, considering the circular dichroism data. As a matter of fact, the incorporation of amphiphilic α helices bearing electrical charges perpendicular to a bilayer requires the helices to associate and to form bundles with the hydrophilic parts facing each other and the hydrophobic ones in contact with the alkyl chains of the bilayer (Cohen & Parry, 1986, 1990). Such an occurrence should involve the ellipticity θ_{222} to be more than 33 000 (the normal value for a single α helix). In all our experiments such a result has never been observed.

(*g*) *Proton NMR*. A ^1H NMR spectrum of vesicles is presented in the insert of Figure 9. The main peaks are assigned as follows: 0.9 ppm, terminal methyl groups; 1.3 ppm, methylene residues; 3.3 ppm, choline methyl groups. The choline methyl signal is a superposition of two components originating from the extravesicular head groups and intravesicular groups. The addition of peptide to the suspension

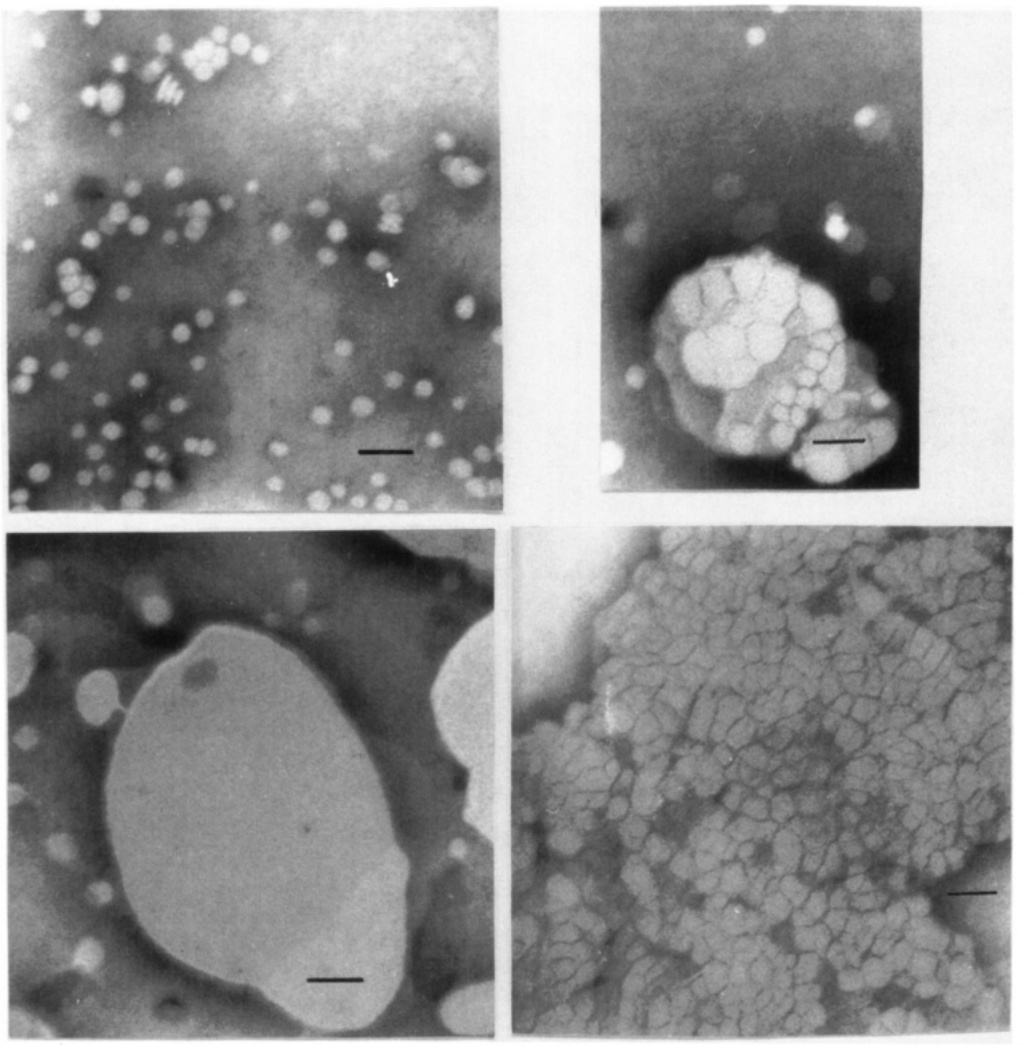

FIGURE 4: Electron microscopy of $(LKKL)_4$ in the presence of DMPC vesicle suspensions for different p values: (a, top left) DMPC vesicle suspension in water; (b, top right) $p = 0.02$; (c, bottom left) $p = 0.05$; (d, bottom right) $p = 0.2$. Bar represents 500 Å.

caused the first peak to move downfield; the two signals coalesced when p reached a value near 0.05. The inside and outside choline methyls thus become magnetically equivalent. A similar behavior has been described for large vesicles by Brouillette et al. (1982); it is related to the fusions observed in this range of p values, in agreement with the conclusions inferred from electron microscopy and turbidimetry.

The line width at half-height of the methyl choline signals remained constant when p varied (Figure 9), showing that the mobility of the corresponding protons was not significantly altered by the peptide/vesicle interaction. The same parameter ($L_{1/2}$) is plotted, as a function of p, in Figure 9 for two other lines, assigned to alkyl methylenes and terminal methyls. The increase in line widths is probably related to an increase of the correlation time. In the range $0 < p < 0.05$ where fusions occur, the decrease in mobility can be related to two factors: (i) increase in vesicle size, leading to incomplete averaging of dipole–dipole interactions through lateral diffusion, and (ii) decreased local mobility of the acyl chains due to formation of a peptide–phospholipid interaction. When $p > 0.05$, that is, in the clearing region, the former effect should disappear.

When vesicles are stepwise added to a $(YKKY)_n$ solution, the intensity of the aromatic proton signals (6.9 and 7.1 ppm) progressively diminishes and finally vanishes for $p = 0.05$. This suggests that freely rotating tyrosyl moieties are progressively replaced by strongly hindered groups, the exchange between the two classes being slow on the NMR time scale.

(*h*) *Phosphorus NMR.* The ^{31}P NMR spectra of vesicles, in the presence of increasing concentrations of peptide, are shown in Figure 10a. The same factors that determine proton line widths should also apply to ^{31}P NMR. The interpretation of the results is, however, complicated by the occurrence of two relaxation mechanisms, the chemical shift anisotropy (CSA) and the dipolar interaction with neighboring protons. On the basis of published results (Tauskela & Thompson, 1992), we estimate that the CSA mechanism accounts for about 80% of the broadening process. Further, the phosphatidylcholine head groups exhibit many different motions (Dufourc et al., 1992), the fastest being a free rotation around the P–O–glycerol bond. Our present results do not allow for a very detailed interpretation; following Tauskela and Thompson (1992), we assume that the reorientation of the phosphate group may adequately be described by a single, isotropic correlation time. As the peptide fraction increases, up to $p \approx 0.05$, phospholipids are found in structures of ever larger sizes. Lateral diffusion will become less and less effective in averaging out the CSA (and also the smaller dipolar contribution). When p becomes larger than 0.05, in the clearing region the structures comprising phospholipids become much smaller, and one would expect the line shape to change and the line width to decrease. On the contrary, these small rigid structures display a long correlation time and broad lines as shown in Figure 10b. The corresponding line width continuously increased when p varied, suggesting progressive

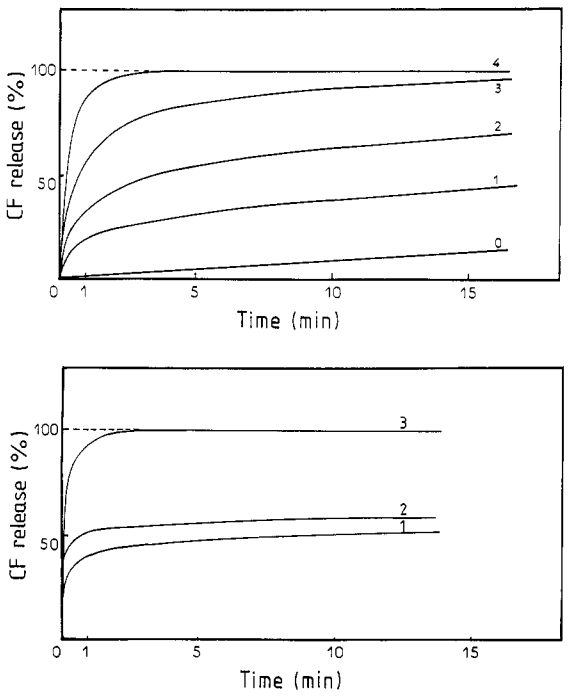

FIGURE 5: Peptide-induced carboxyfluorescein leakage at pH 7.4 from DMPC vesicles. (a, top) Time course of CF efflux in the presence of $(LKKL)_4$: (0) $p = 0$, free DMPC vesicles; (1) $p = 0.04$; (2) $p = 0.09$; (3) $p = 0.19$; (4) 50 μL of Triton X-100 at 1% in 2 mL. (b, bottom) Time course of CF efflux in the presence of $(YKKY)_n$: (1) $p = 0.04$; (2) $p = 0.09$; (3) 50 μL of Triton X-100 at 1% in 2 mL.

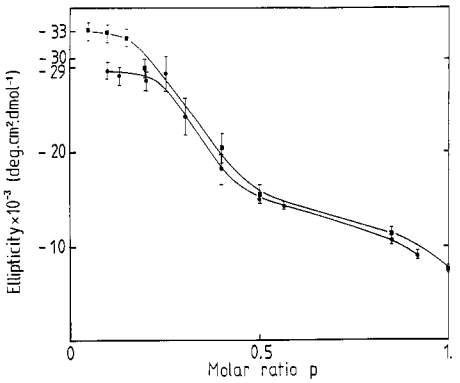

FIGURE 6: Mean residue ellipticity variation with p: (■) $(LKKL)_4$; (●) $(LKKL)_n$. Measurements were made at 208 nm in an aqueous suspension of SUV vesicles and peptides at 30 °C.

weakening of the phosphorus atom mobility around the P–O–glycerol bond. The total phosphorus intensity corrected for dilution effect remained constant within the margin of experimental error (less than 10%) as shown in Figure 10b; thus NMR spectra can be taken as representative of the whole sample.

When the plot of line width against p is extrapolated toward increasing p, it can be pointed out that the limit value of p, near 0.3, roughly corresponds to that determined by circular dichroism concerning the average complexation number. Such a result suggests the immobilization of most phosphorus atoms when p is higher than 0.3.

(*i*) *Fluorescence Study of* $(YKKY)_n$. In order to gain further information on the location of the hydrophobic part of the peptides in lipid bilayers, we have examined the fluorescence of tyrosyl residues in $(YKKY)_n$. Figure 11 displays fluorescence spectra of $(YKKY)_n$ at two different concentrations in water (Curves 1′ and 2′), in 0.15 M sodium perchlorate (curves 1″ and 2″), and in 4.92×10^{-2} M DMPC vesicle suspension.

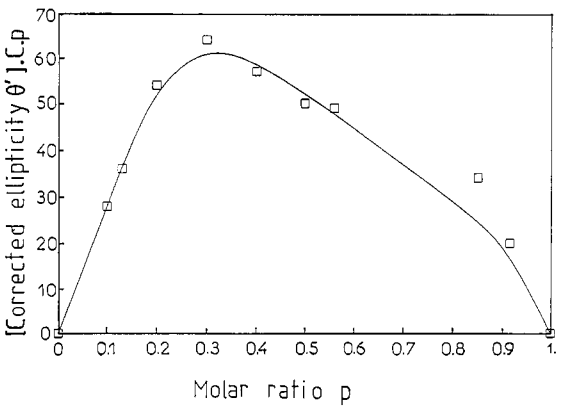

FIGURE 7: Corrected ellipticity of $(LKKL)_4$ plotted against p (see Appendix I). The curve comes through a maximum near $p = 0.33$. This value corresponds to the average complexation number $n = 2$ (i.e., one amino acid residue for two phospholipid molecules on average).

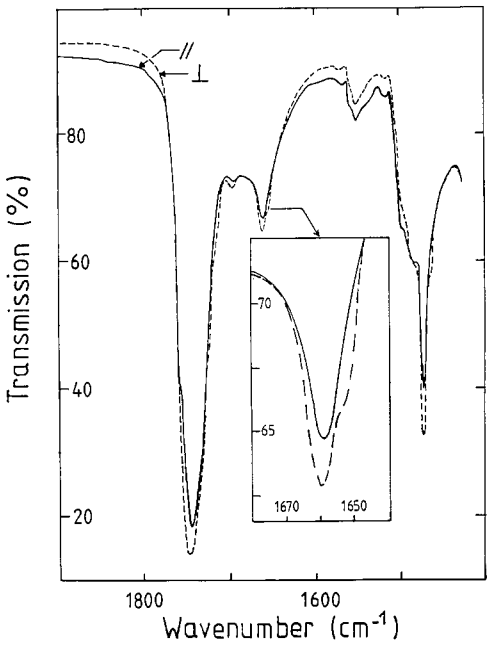

FIGURE 8: Infrared dichroism of $Ac(LKKL)_4NHEt$ in the presence of DMPC vesicles. Molar ratio $p = 0.09$. Absorption of amide band I: (—) $A_{\parallel}$; (- - -) $A_{\perp}$. Insert: amide I band magnified.

No difference was observed between spectra for peptides in water and in sodium perchlorate where $(YKKY)_n$ is assumed to adopt an α-helical conformation.

In the presence of DMPC vesicles (see curves 1 and 2) the emission maximum experienced no blue shift, as expected for tyrosyl residues when the environment polarity was modified (in contrast with the situation of tryptophan). However, the fluorescence intensity increased and was multiplied by a factor of 2.5. As pointed out by Azzi (1975), a high quantum yield may be due not only to the absence of polar molecules but also to the shielding from quenchers or to particular geometries imposed by constraints upon the fluorochrome. In the case of $(YKKY)_n$ it stands to reason that the actual effect was consistent with a decrease of the polarity of the tyrosyl environment which can be explained by a direct interaction of this residue with the hydrophobic core of DMPC vesicles. According to Cowgill (1967) the observed variation of such a quantum yield would correspond to a polarity comparable to a macroscopic dielectric constant of about 17. This means that tyrosyl residues can penetrate into the outer phospholipid

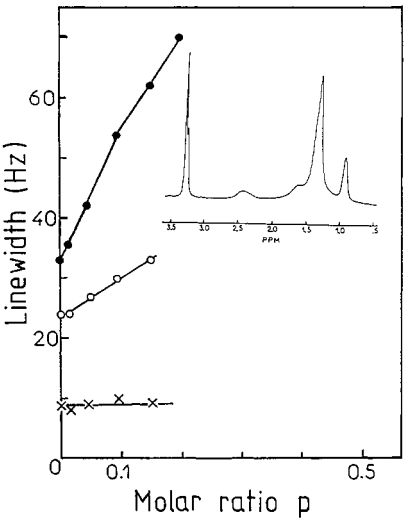

FIGURE 9: ^{1}H NMR line width at half-height dependence with p of choline methyl protons (×), methylene (○), and terminal methyl groups (●) of DMPC vesicles in the presence of $(LKKL)_4$. Vesicle concentration = 4.95×10^{-2} M. Insert: NMR spectrum of SUV in D_2O.

layer up to nearly the level of carbon 4 or 5 (Israelachvili et al., 1980).

(j) Modeling and Energy Calculations of Possible Ac(LKKL)$_4$NHEt–DMPC Complexes: Direct Interactions between Lipid Molecules and Amino Acid Residues. (i) Starting Conformations. Modeling and energy calculations were carried out on the basis of experimental results. Our main conclusions are recalled as follows:

(1) The anchoring sites of the polypeptide on DMPC molecules are the negative phosphate groups through electrostatic interactions with the positive NH_3^+ groups of lysine residues.

(2) The polypeptide adopts an α-helical conformation with its axis parallel to the membrane surface. The hydrophobic part of the amphiphilic α helix can penetrate the outer lipid leaflet down to the C_4 position [the behavior of the leucine residues in $(LKKL)_4$ is likely to mimic that of tyrosyl residues in $(YKKY)_n$].

(3) Choline methyl groups are not involved in the interactions between lipid molecules and amino acid residues.

(4) Phosphorus atom mobility around the P–O–glycerol bond is strongly reduced, whereas that of methylene groups is progressively weakened when going up from C_{13} to C_1.

The starting conformations of the different possible complexes were built up in three steps as follows:

(1) The flexible lysine chains of the polypeptide were kept either straight or folded and brought into close contact by dummy constraints that will be removed in the latest steps of energy minimization. In the schematic representation of Figure 12, (1) corresponds to stretched lysine side chains and (2) and (3) to the folded side chains (i) and (i+1), and (i) and (i+4), respectively (i denotes the numbering of the lysine residues). A last possibility, (i) and (i+5) folding, is ruled out because the corresponding amino acid residues are too far apart.

(2) Two models for starting conformations of a DMPC molecule were considered: (I) with two interacting alkyl chains and (II) with independent chains (the roman numerals refer to lipid molecules).

(3) Ac(LKKL)$_4$NHEt was anchored to the phosphate group of a single lipid molecule and viewed on a screen. Three possible types of complexes resulted from the association of one lipid (I) with any polypeptide model, (1), (2), or (3). In contrast, the lipid with independent chains (II) was only accommodated by (2). In the following, complex A refers to [I, (1)], complex B to [I, (2)], complex C to [I, (3)], and complex D to [II, (2)] association.

(ii) Energy Calculations. Energy calculations were processed as indicated under Materials and Methods.

The starting conformations were built by considering the association of a single lipid molecule with the polypeptide. As a matter of fact, preliminary calculations with one to four lipid molecules have shown that the energies were additive, and therefore the reasoning could be conducted taking into account a single phospholipid molecule anchored to the α helix. Unless otherwise stated, for the sake of clarity and computational time saving, we studied the complexes with a single lipid molecule anchored to the α helix.

The energies of each complex, A–D, were minimized using the Powell method. The computation methodology involved four steps. First the polypeptide was made rigid. In the second step the lysine side chains were made flexible. In the third step only the helical skeleton was kept rigid. Finally, all

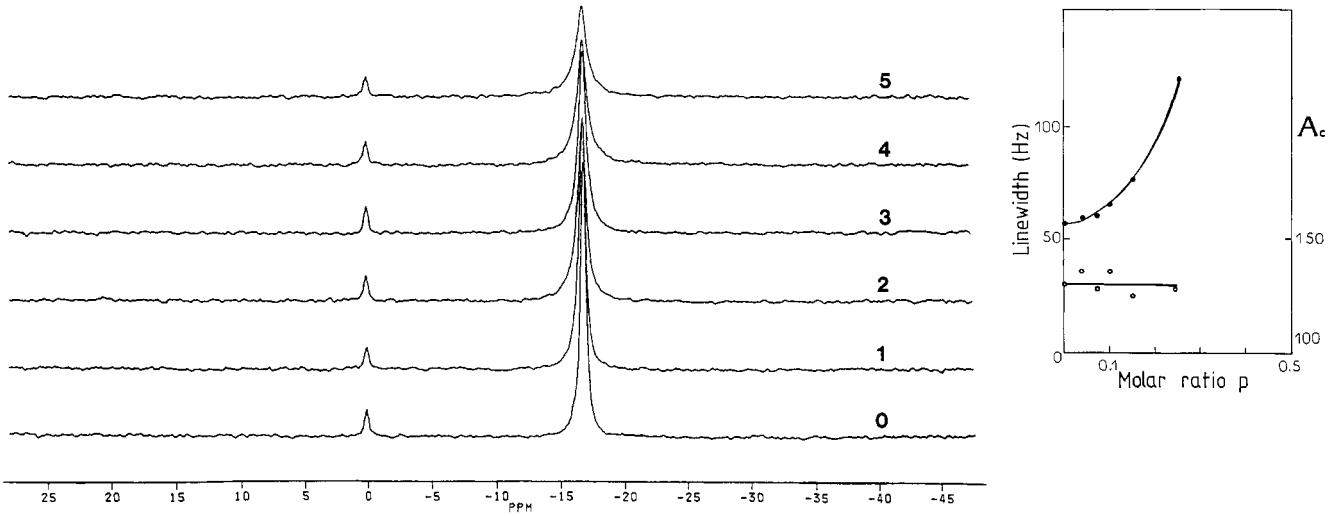

FIGURE 10: (a, left) ^{31}P NMR spectra of DMPC vesicles in the presence of Ac(LKKL)$_4$NHEt. p = molar ratio. Curves: (0) p = 0, free DMPC vesicles; (1) p = 0.04; (2) p = 0.07; (3) p = 0.1; (4) p = 0.15; (5) p = 0.25. The reference (0 ppm) was methylenediphosphonic acid; 2000 scans were accumulated for each spectrum. (b, right) (●) Variation of the line width derived from ^{31}P NMR spectra with p. (○) Variation of the corrected phosphorus intensity A_c (in arbitrary units) with p.

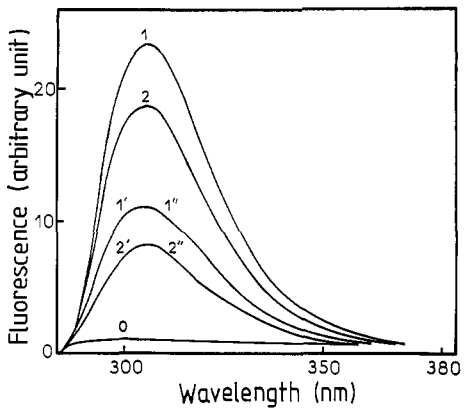

FIGURE 11: Fluorescence spectra for $(YKKY)_n$: in water, (1') p = 0.05 and (2') p = 0.025; in 0.15 M $NaClO_4$, (1'') p = 0.05 and (2'') p = 0.025; in the presence of DMPC vesicles, (1) p = 0.05 and (2) p = 0.025; (0) pure DMPC vesicles. Quantum yield = 2.5.

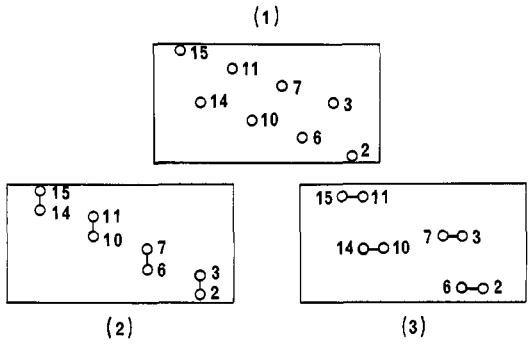

FIGURE 12: Scheme of possible lysine side-chain foldings when a phospholipid molecule is anchored with an α-helix polypeptide. The figures associated to the open circles refer to the numbering of the lysine residues, and the solid lines refer to the anchoring sites.

Table II: Minima of Interaction Energies and Percentage of the van der Waals Interaction Energy[a]

complex	E_T (kcal·mol^{-1})	E_P (kcal·mol^{-1})	E_L (kcal·mol^{-1})	ΔE (kcal·mol^{-1})	E_{chain} (%)
A	−1.7	9.4	15.0	−26.1	27
B	9.5	49.3	12.3	−52.1	28
C	32.6	61.3	13.1	−41.8	58
D	5.8	51.8	28.8	−74.8	36

[a] E_T, total energy of successive complexes; E_P, intramolecular energy of the α helix; E_L, intramolecular energy of a DMPC molecule; ΔE, interaction energy; E_{chain}, van der Waals interaction energy of alkyl chains with the α helix.

distance constraints were removed, and the minimization led to the total energy E_T.

The interaction energy ΔE was given by the relationship $\Delta E = E_T - (E_p + E_L)$, where E_p and E_L are respectively the polypeptide and lipid intramolecular energy in the complex.

(iii) Results. The energy values for complexes A–D are summarized in Table II, and the corresponding conformations are shown in Figure 13.

The lowest energy complex, D (Figure 13d), is the one with the K_i and K_{i+1} folded residues and the independent alkyl chains mounting the helix as a rider does. The mean direction between the glycerol C_2 and the phosphorus atom is parallel to the helix axis, and the choline head protrudes outward. The longest alkyl chain comes into the helix groove between L_{i-1}, L_{i+3} whereas the other one does in the same way on the other side between L_{i-2}, L_{i+2}. The shortest distances between the methylene protons and leucine C_δ occur at the level of C_{11} to C_{13}.

The second energy minimum occurs for complex B (Figure 13b) with the same polypeptide conformation (i.e., K_i, K_{i+1} folding) and the two lipid chains located on the same side of the α helix. In this complex, the glycerol group lies in a plane perpendicular to the helix axis, and the choline head protrudes outward. The two alkyl chains are inserted in two grooves between L_{i-5}, L_{i-1} and L_{i-1}, L_{i+3}. The closest contacts with L_{i-1} occur with C_{10} to C_{13} and L_{i+3} with C_6 to C_9.

Complex C (Figure 13c) corresponds to a different folding of lysine chains between K_i and K_{i+4}. The lipid molecules are spread in the same grooves as in complex B, but the closest contacts with leucine residues take place at the C_4 or C_5 level. The alkyl chains being able to move more freely, the negative interaction energy is higher than those of complexes B and D.

Complex A (Figure 13a) has the highest interaction energy. In this model, the lysine side chains are stretched; one lipid molecule interacts with one NH_3^+ lysine residue. One alkyl chain is free and does not set on interaction with any amino acid residue whereas the shortest one is inserted in the L_{i-5}, L_{i-1} groove. Thus, the mobility of this chain is mainly constrained at the C_3 or C_4 level. In addition, electrostatic and van der Waals interactions are weakened (Table II).

CONCLUSION

Considering the energy minima, the four models displayed in Figure 13 are likely to exist. Nevertheless, examination of the results of the comprehensive experimental study enables us to select complex C as the most probable one.

As a matter of fact, in model D (Figure 13d) the motions of the methylene and terminal methyl protons are more reduced than in the other three complexes. The α helix is indeed more deeply embedded into the outer lipid leaflet, which is not consistent with the ^1H NMR and fluorescence results.

As for complex A, the electrostatic binding energy of the lipid phosphate group to the ammonium lysine group is only −15 kcal·mol^{-1}, whereas it is respectively −23.4, −24.9, and −27.9 kcal·mol^{-1} for complexes B, C, and D. This suggests less restricted motions of the phosphorus atom in complex A, in contradiction with the ^{31}P NMR results.

Finally, the chain van der Waals energy (Table II) is higher in complex C than in complex B. Besides, the averaged C_4 level of maximum interaction between hydrophobic residues and alkyl chains with complex C is in better agreement with the conclusion of the fluorescence experiments.

All these arguments are in favor of the choice of complex C as the most probable model. Therefore, Figure 14 exhibits the minimized structure of the complex with four lipid molecules in direct interaction with the α helix. The interaction energy for this structure is −160.1 kcal·mol^{-1}, which is nearly four times the interaction energy of complex C with one lipid (−41.8 kcal·mol^{-1}). However, considering the experimental value of the average complexation number (two lipids per amino acid), such a structure should be completed by adding other lipid molecules around the α helix. These molecules could be maintained in a ring-shaped configuration through the electric field lines generated by the α-helix macrodipole (Reynaud, 1988). As a matter of fact, the α helix can be considered as a large permanent macrodipole arising from the alignment of peptide dipoles. A commonly accepted value for the peptide unit dipole moment is 3.6 D (Pethig, 1979). The electrostatic effect of the α helix is roughly equivalent to the effect of two partial charges of opposite sign (0.8 electronic charge) placed at the ends of the α helix (Pethig, 1979; Hol, 1985). The hydrophobic core of phospholipid bilayers has a

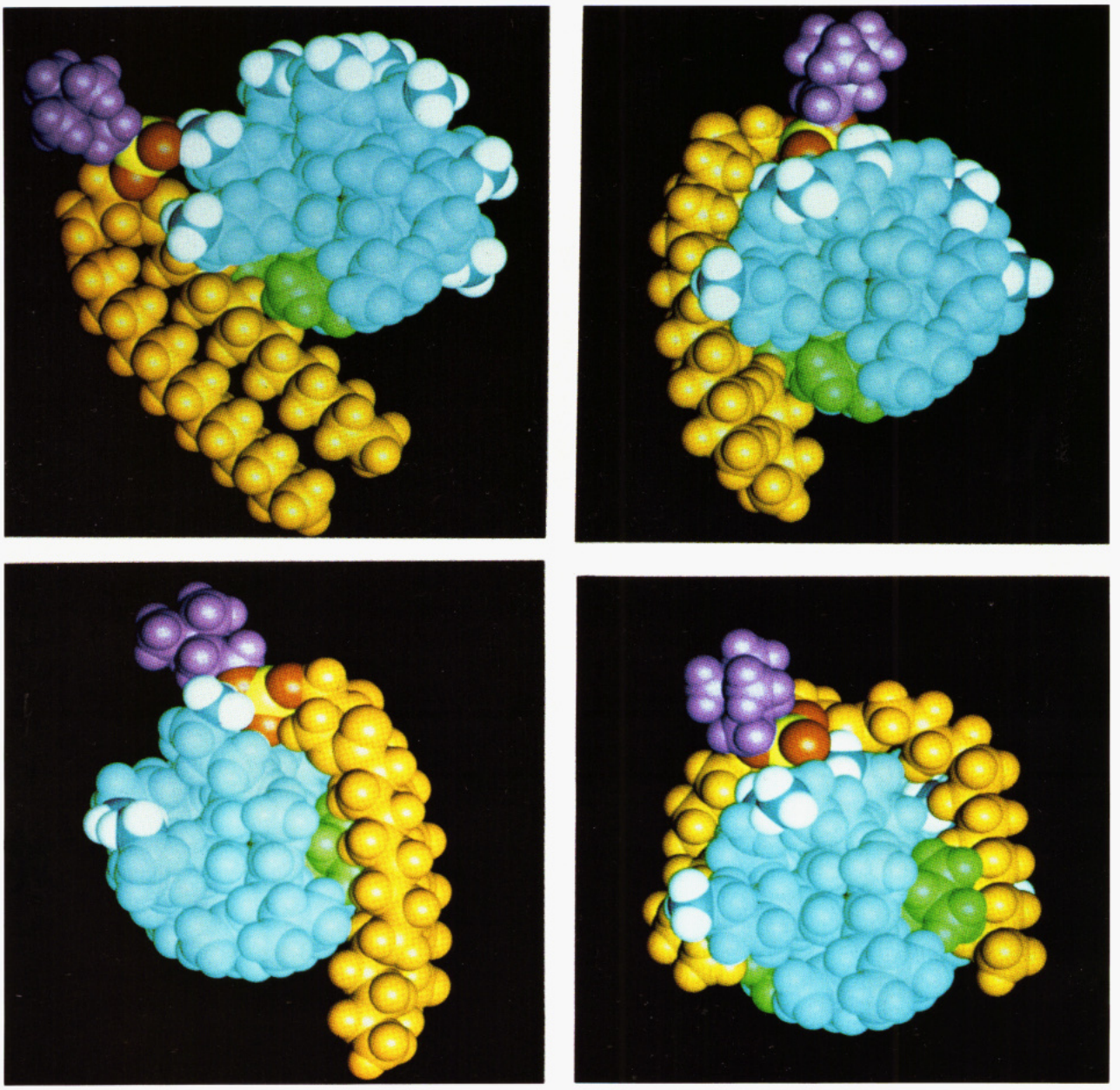

FIGURE 13: The four complex models (axial view). The α helix is in light blue except for the lysine NH_3^+ (dark blue nitrogen and white hydrogen atoms). Hydrophobic amino acid residues in strong interaction with the adjacent alkyl chains are green. Lipid molecules are in orange but phosphate groups are colored by atom type (phosphorus in yellow; oxygen in red) and choline heads are purple. Panels: (a, top left) complex A; (b, top right) complex B; (c, bottom left) complex C; (d, bottom right) complex D.

low permittivity. This means that charges held within biological membranes create large electric fields **E** around them (Brown, 1990). These fields may be felt by neighboring phospholipid heads, the dipole moment of which, μ, is estimated to be 18.7 D (Shepherd & Boldt, 1978). The size of the field around the α helix at the level of phospholipid heads can be computed from electrostatic theory using the method of images. Such a calculation (Reynaud, unpublished results) was carried out by assuming that the charges at the ends of the α helix were in an homogeneous thin slab of permittivity 20 [see Fluorescence Study of $(YKKY)_n$ in this paper] and phospholipid head groups in an adjacent slab of permittivity 30 (Israellachivili et al., 1980). The potential energy $-\mu\cdot\mathbf{E}$ of each phospholipid dipole neighboring the α helix was compared to the thermal agitation kT, and from Langevin's theory (Pethig, 1979) the average moment $\langle\mu\rangle$ per dipole in the direction of the field was determined. In Figure 15, the lipid assembly around the $(LKKL)_4$ helix is drawn to scale in the case of model C. The cross section (a) parallel to the bilayer contains the phosphorus atoms while (b) is perpendicular to the bilayer and contains the α-helix axis.

Phospholipid head groups oriented by the electric field were represented by open circles of 55-Å^2 area and the four in direct interaction with amino acid residues by shaded circles.

The α helix is schematized by a rectangle of dimensions 24 Å × 12 Å and $\langle\mu\rangle$ by an arrow, the length of which is proportional to its calculated value. Such a representation shows that, in addition to the 4 phospholipid molecules in direct interaction with the α helix, about 20 molecules mainly located at the helix ends can be field-oriented and, so, give rise to a ring-shaped domain around the peptide. It should be pointed out that the number of field-oriented phospholipid head groups is probably underestimated for the following reasons: first, the field-oriented head-group area is certainly

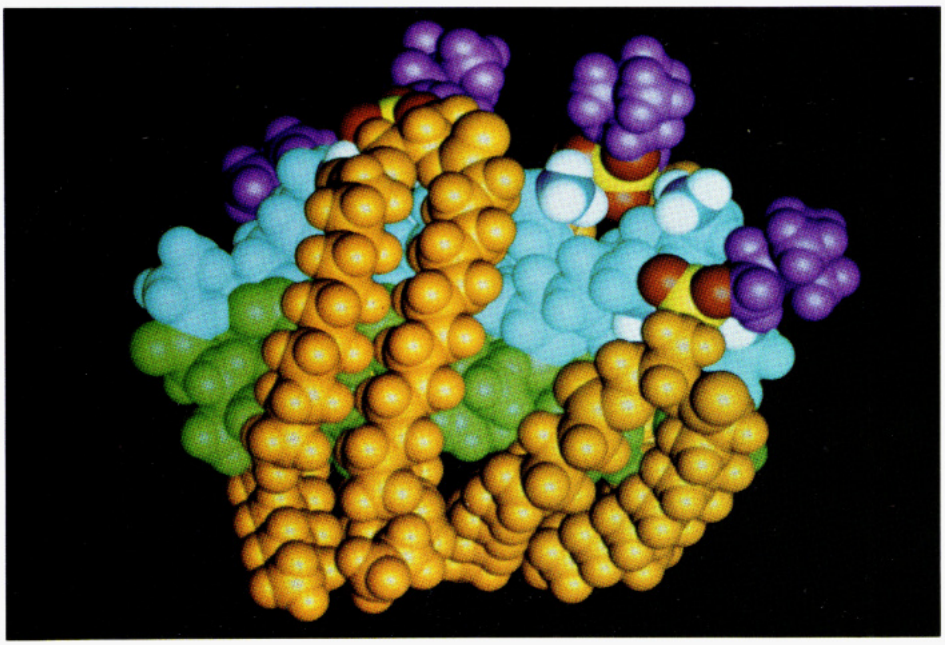

FIGURE 14: Complex C with four lipid molecules in interaction with Ac(LKKL)$_4$NHEt (side view).

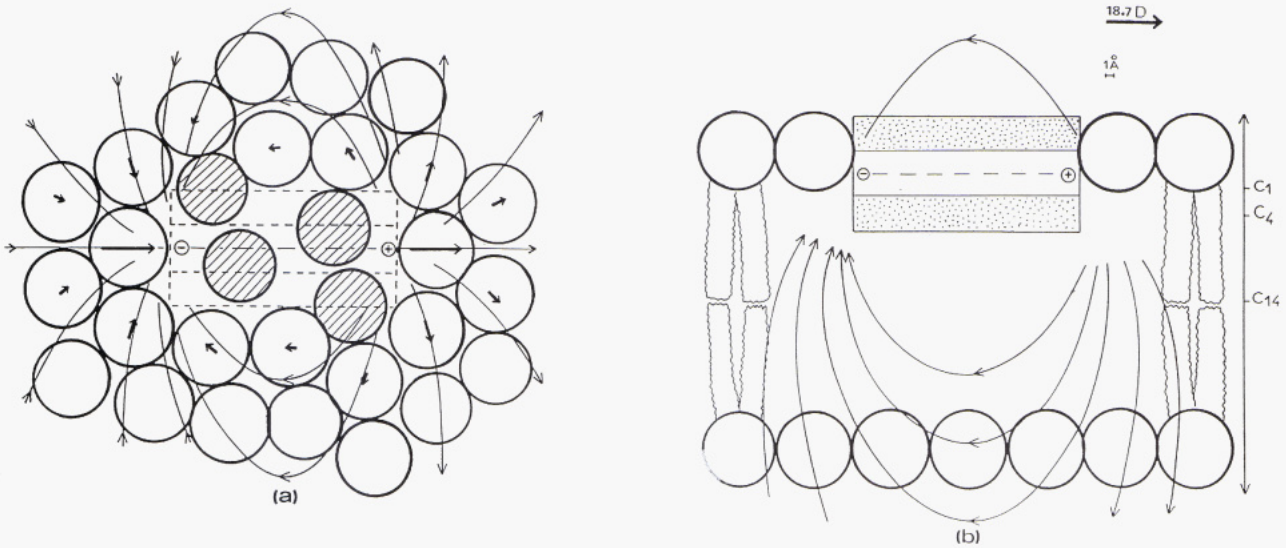

FIGURE 15: (LKKL)$_4$ α helix interacting with a bilayer drawn to scale: (open circles) phospholipid head groups, area 55 Å^2; (shaded circles) phospholipid head groups in direct interaction with the α helix; (solid arrows) average moment $\langle\mu\rangle$ per phospholipid head dipole in the direction of the field, the length of which is proportional to its value (Debye unit); (rectangle) schematic of the α helix; (thin lines) lines of force in the electric field of an α helix; (dotted area) amino acid side-chain area. Panels: (a) cross section parallel to the bilayer and containing phosphorus atoms; (b) cross section perpendicular to the bilayer and containing α-helix axis.

less than 55 Å^2; second, as shown by Lockhart and Kim (1992) and Hol (1985), the dipole moment of an α helix is larger than that based upon a single addition of static peptide dipoles.

In conclusion, we think that the proposed model of interaction between a lipid bilayer and an amphiphilic peptide like (LKKL)$_4$ is in agreement with the experimental data and can help us understand the properties of natural amphiphilic peptides interacting with biological membranes. Particularly, pore formation and fusogenic properties are taken into account by this model, the occurrence of structured domain boundaries being the points at which pore formation and/or membrane intermixing between adhering vesicles can take place (Blumenthal, 1987; Papahadjopoulos et al., 1990).

It should be pointed out that this model is different from those developed by other authors (Edholm & Jähnig, 1988; Wang & Pullman, 1991), whose works concern the modeling of hydrophobic membrane-spanning α helices. Particularly, in the case of Ac(LKKL)$_4$NHEt, the hydrophobicity gradient is perpendicular to the α-helix axis which is located parallel to the bilayer and penetrates the outer lipid leaflet without giving rise to any helix bundle.

ACKNOWLEDGMENT

We thank Dr. A. Brack and D. Lelievre for the gift of polymers I, III, and IV used in this study.

APPENDIX I: JOB'S METHOD—COMPLEXATION NUMBER DETERMINATION

Let us mix equimolecular solutions of the two components, A and Z, which can bind each other and lead to the formation of a complex, X, as follows:

$$A + nZ \rightleftarrows X \qquad (1)$$

Let C be the common concentration of the solutions and p the molar ratio of A in the different mixtures.

We can write a set of three equations from (1)

$$[A][Z]^n = K_D[X] \quad (2)$$

$$[Z]_{total} = [Z] + n[X] = (1-p)C \quad (3)$$

$$[A]_{total} = [A] + [X] = pC \quad (4)$$

with K_D = dissociation constant, [A] = molar concentration of A, [Z] = molar concentration of Z, and [X] = molar concentration of X.

Now let us determine the value p which makes the complex concentration [X] be maximum. For that let us differentiate (2), (3), and (4) with respect to p and write

$$\frac{d[X]}{dp} = 0$$

$$[A]n[Z]^{n-1}\frac{d[Z]}{dp} + [Z]^n\frac{d[A]}{dp} = 0 \quad (5)$$

$$\frac{d[Z]}{dp} = -C$$

and

$$\frac{d[A]}{dp} = C$$

After replacement of $d[A]/dp$ and $d[Z]/dp$ by C and $-C$ and rearrangement of (5), we obtain

$$-[A]n + [Z] = 0 \quad (6)$$

By combining (3), (4), and (6), the final relationship between n and p becomes

$$n = \frac{1-p_m}{p_m}$$

APPENDIX II: IR DICHROIC RATIO FOR PARTIALLY ORIENTED α HELICES

The amide I transition moment is assumed to lie at an angle α from the helix axis; the transition moments are uniformly distributed around the helix axis. The light is incident in the (Y, Z) plane, in a direction at angle r from the Z axis normal to the disk. This value may be computed from the known angle of incidence i using Descartes' law: $\sin i = n \sin r$.

Case I: *Random Orientation in a Plane.* A reference helix is located along the X axis, with the transition moment in the (X, Z) plane. The transition dipole thus has components ($M \cos \alpha$, 0, $M \sin \alpha$). A general orientation of the dipole is generated by two consecutive rotations: rotation of angle ω with respect to OX, followed by a rotation of angle ψ with respect to OZ. The transition dipole is then

$$M\begin{bmatrix} \cos\psi\cos\alpha + \sin\omega\sin\psi\sin\alpha \\ \sin\psi\cos\alpha - \sin\omega\cos\psi\sin\alpha \\ \cos\omega\sin\alpha \end{bmatrix}$$

The electric field is either $\mathbf{E}_\parallel = [0, E\cos r, E\sin r]$ or $\mathbf{E}_\perp = [E, 0, 0]$. The absorption coefficients are $A_\parallel = [\mathbf{E}_\parallel \cdot \mathbf{M}]^2$ and $A_\perp = [\mathbf{E}_\perp \cdot \mathbf{M}]^2$, for a given dipole orientation. The observed absorption coefficients are the mean values of the A's over all possible angles ω and ψ.

Straightforward algebra yields

$$\langle A_\parallel \rangle = \left[\frac{1}{2}\cos^2 r\cos^2\alpha + \frac{1}{4}\sin^2\alpha\,(2-\cos^2 r)\right][EM]^2$$

$$\langle A_\perp \rangle = \left[\frac{1}{4}(1+\cos^2\alpha)\right][EM]^2$$

from which the dichroic ratio follows:

$$D_I = \frac{\langle A_\parallel \rangle}{\langle A_\perp \rangle} = \frac{(3\cos^2\alpha - 1)\cos^2 r + 2\sin^2\alpha}{1+\cos^2\alpha}$$

For the commonly accepted $\alpha = 39°$, D is always <1.

Case II: *Helices Normal to a Plane.* The reference helix is now parallel to OZ, with the transition moment in the (X, Z) plane, so that the dipole is $[M\sin\alpha, 0, M\cos\alpha]$. A general orientation is obtained following a rotation of ψ about OZ, resulting in dipole components

$$M\begin{bmatrix} \sin\alpha\cos\psi \\ \sin\alpha\sin\psi \\ \cos\alpha \end{bmatrix}$$

from which one can easily derive

$$\langle A_\parallel \rangle = \left[\sin^2 r\cos^2\alpha + \frac{1}{2}\cos^2 r\sin^2\alpha\right][EM]^2$$

$$\langle A_\perp \rangle = \frac{1}{2}\sin^2\alpha\,[EM]^2$$

$$D_{II} = \frac{\langle A_\parallel \rangle}{\langle A_\perp \rangle} = 2\sin^2 r\cot^2\alpha + \cos^2 r$$

which is always larger than unity when $\alpha = 39°$.

The calculations summarized above are strictly valid only for an infinitely long, rigid helix. They should be a good approximation for a short peptide.

REFERENCES

Anantharamaiah, G. M., Jones, J. L., Brouillette, C. G., Schmidt, C. F., Chung, B. H., Hughes, T. A., Bhown, A. S., & Segrest, J. P. (1985) *J. Biol. Chem. 260*, 10248–10255.

Azzi, A. (1975) *Q. Rev. Biophys. 8*, 237–316.

Bamford, C. H., Elliott, A., & Hanby, W. E. (1956) *Synthetic Polypeptides*, pp 182–183, Academic Press, New York.

Barbier, B., Perello, M., & Brack, A. (1988) *Collect. Czech. Chem. Commun. 53*, 2825–2832.

Blumenthal, R. (1987) *Curr. Top. Membr. Transp. 29*, 203–254.

Brack, A., & Caille, A. (1978) *Int. J. Pept. Protein Res. 11*, 128–139.

Brasseur, R. (1991) *J. Biol. Chem. 266*, 16120–16127.

Brasseur, R., & Ruysschaert, J. M. (1986) *Biochem. J. 238*, 1–11.

Brouillette, C. G., Segrest, J. P., Thian, C. N., & Jones, J. L. (1982) *Biochemistry 21*, 4569–4575.

Brown, G. C. (1990) *FEBS Lett. 260*, 1–5.

Bruner, J. (1989) *FEBS Lett. 257*, 369–372.

Clague, M. J., Knutson, J. R., Blumenthal, R., & Herrmann, A. (1991) *Biochemistry 30*, 5491–5497.

Clark, M., Cramer, R. D., & Van Opdenbosch, N. (1989) *J. Comput. Chem. 10*, 982–1012.

Cohen, C., & Parry, D. A. D. (1986) *Trends Biochem. Sci. 11*, 245.

Cohen, C., & Parry, D. A. D. (1990) *Proteins: Struct., Funct., Genet. 7*, 1.

Cowgill, R. W. (1967) *Biochim. Biophys. Acta 133*, 6–18.

Dufourc, E. J., Mayer, C., Stohrer, J., Althoff, G., & Kothe, G. (1992) *Biophys. J. 61*, 42–57.

Edholm, O., & Jähnig, F. (1988) *Eur. Biophys. J. 30*, 279–292.

Greenfield, N., & Fasman, G. D. (1969) *Biochemistry 8*, 4108–4116.
Ho, S. P., & De Grado, W. F. (1987) *J. Am. Chem. Soc. 109*, 6751–6758.
Hol, W. J. G. (1985) *Prog. Biophys. Mol. Biol. 45*, 149–195.
Houbre, D., Kuhry, J. G., & Duportail, G. (1988) *Biophys. Chem. 30*, 245–255.
Huang, C. H. (1969) *Biochemistry 8*, 344–352.
Israelachvili, S., Marcelja, S., & Horn, R. G. (1980) *Q. Rev. Biophys. 13*, 121–200.
Kaiser, E. T., & Kezdy, F. J. (1987) *Annu. Rev. Biophys. Chem. 16*, 561–581.
Kato, T., Lee, S., Ono, S., Agawa, Y., Aoyagi, H., Ohno, M., & Nischino, N. (1991) *Biochim. Biophys. Acta 1063*, 191–196.
Kono, K., Kimura, S., & Imanishi, Y. (1990) *Biochemistry 29*, 3631–3637.
Lee, S., Ono, S., Nakamura, M., Aoyagi, H., & Kato, T. (1987) in *Peptide Chemistry* (Shiba T., & Sakakibara, S., Eds.) pp 49–52, Protein Research Foundation, Minoh-shi, Osaka, Japan.
Lee, S., Aoki, R., Oishi, O., Aoyagi, H., & Yamasaki, N. (1992) *Biochim. Biophys. Acta 1103*, 157–162.
Lockhart, D. J., & Kim, P. S. (1992) *Science 257*, 947–951.
Mac Lean, L., Hagaman, A. K., Owen, J. T., & Krstenansky, J. L. (1991) *Biochemistry 30*, 31–37.
Maget-Dana, R., & Trudelle, Y. (1991) in *Proceedings of the 4th Colloquium, Molecules and membrane interaction*, University of Strasbourg, Strasbourg, France.
Merulka, G., & Stellwagen, E. (1991) *Biochemistry 30*, 4245–4248.
Mihara, H., Kanmera, T., Yoshida, M., Lee, S., Aoyagi, H., Kato, T., & Izumiya, N. (1987) *Chem. Soc. Jpn. 60*, 697–706.
Mosior, M., & McLaughlin, S. (1992) *Biochemistry 31*, 1767–1773.
Nabedryk, E., Gingold, H. P., & Breton, J. (1982) *Biophys. J. 38*, 243–249.
Ono, S., Suenaga, M., Lee, S., & Aoyagi, H. (1988) in *Peptide Chemistry* (Ueki, M., Ed.) pp 307–312, Protein Research Foundation, Minoh-shi, Osaka, Japan.
Ono, S., Lee, S., Mihara, M., Aoyagi, H., Kato, T., & Yamasakin, N. (1990) *Biochim. Biophys. Acta 1022*, 237–244.
Papahadjopoulos, D., Nir, S., & Düzgünes, N. (1990) *J. Bioenerg. Biomembr. 22*, 157–179.
Perello, M., Barbier, B., & Brack, A. (1991) *Int. J. Pept. Protein Res. 38*, 154–160.
Pethig, R. (1979) *Dielectric and Electronic Properties of Biological Materials*, John Wiley and Sons, New York.
Reynaud, J. A. (1988) *Proceedings of the 3rd Colloquium of Bioelectrochemistry*, CNRS ed., Orléans, France.
Reynaud, J. A., Brack, A., Grivet, J. P., & Trudelle, Y. (1990) in *Peptides* (Giralt, E., & Andreu, D., Eds.) p 490, ESCOM Science Publishers B.V., Leiden, The Netherlands.
Schlegel, R., & Wade, M. (1985) *J. Biol. Chem. 260*, 4691–4694.
Shepherd, J., & Boldt, G. (1978) *Biochim. Biophys. Acta 514*, 83–94.
Souchay, P. (1961) *Thermodynamique Chimique*, Masson, Paris.
Suenaga, M., Lee, S., Aoyagi, H., & Kato, T. (1988) in *Peptide Chemistry* (Ueki, M., Ed.) pp 301–306, Protein Research Foundation, Minoh-shi, Osaka, Japan.
Surewicz, W. K., & Epand, R. M. (1984) *Biochemistry 23*, 6072–6077.
Takahashi, S. (1990) *Biochemistry 29*, 6257–6263.
Tamm, L. K. (1991) *Biochim. Biophys. Acta 1071*, 123–148.
Tauskela, J. S., & Thompson, M. (1992) *Biochim. Biophys. Acta 1104*, 137–146.
Taylor, J. W., & Osapay, G. (1990) *Acc. Chem. Res. 23*, 10.
Trudelle, Y. (1975) *Polymer 16*, 9–15.
Trudelle, Y., & Spach, G. (1975) *Polymer 16*, 16–20.
Wang, J., & Pullman, A. (1991) *Biochim. Biophys. Acta 1070*, 493–496.
Weinstein, J. N., Yoshikami, S., Henkart, P., Blumenthal, R., & Hagins, W. A. (1977) *Science 195*, 489–492.
Woody, R. W. (1978) *Biopolymers 17*, 1451–1467.
Yeagle, P. L., Epand, R. M., Richardson, C. D., & Flanagan, T. D. (1991) *Biochim. Biophys. Acta 1065*, 49–53.